PHOTONICS Research

Circular dichroism-like response of terahertz wave caused by phase manipulation via all-silicon metasurface

Jie Li,[1,†] Chenglong Zheng,[1,†] Guocui Wang,[2,3] Jitao Li,[1] Hongliang Zhao,[1] Yue Yang,[1] Zhang Zhang,[1] Maosheng Yang,[4] Liang Wu,[1] Jining Li,[1] Yating Zhang,[1,5] Yan Zhang,[2] and Jianquan Yao[1,6]

[1]Key Laboratory of Opto-Electronics Information Technology (Tianjin University), Ministry of Education, School of Precision Instruments and Opto-Electronics Engineering, Tianjin University, Tianjin 300072, China
[2]Beijing Key Laboratory for Metamaterials and Devices, Key Laboratory of Terahertz Optoelectronics, Ministry of Education, and Beijing Advanced Innovation Center for Imaging Technology, Department of Physics, Capital Normal University, Beijing 100048, China
[3]Beijing Engineering Research Center for Mixed Reality and Advanced Display, School of Optics and Photonics, Beijing Institute of Technology, Beijing 100081, China
[4]School of Mechanical Engineering, Jiangsu University, Zhenjiang 225009, China
[5]e-mail: yating@tju.edu.cn
[6]e-mail: jqyao@tju.edu.cn

Received 20 November 2020; revised 1 February 2021; accepted 7 February 2021; posted 8 February 2021 (Doc. ID 415547); published 26 March 2021

Chiral metasurfaces based on asymmetric meta-atoms have achieved artificial circular dichroism (CD), spin-dependent wavefront control, near-field imaging, and other spin-related electromagnetic control. In this paper, we propose and experimentally verify a scheme for achieving high-efficiency chiral response similar to CD of terahertz (THz) wave via phase manipulation. By introducing the geometric phase and dynamic phase in an all-silicon metasurface, the spin-decoupled terahertz transmission is obtained. The giant circular dichroism-like effect in the transmission spectrum is observed by using a random phase distribution for one of the circular polarization components. More importantly, the effect can be adjusted when we change the area of the metasurface illuminated by an incident terahertz beam. In addition, we also demonstrate the spin-dependent arbitrary wavefront control of the transmitted terahertz wave, in which one of the circularly polarized components is scattered, while the other forms a focused vortex beam. Simulated and experimental results show that this method provides a new idea for spin selective control of THz waves.

https://doi.org/10.1364/PRJ.415547

1. INTRODUCTION

Chirality is a special geometric asymmetry in nature, which exists widely in microscopic matter and macroscopic objects [1]. The chiral structure of the optical medium may trigger a chiral optical response, which can be explained as different refractive indices for left- and right-handed circularly polarized (LCP and RCP) light [2]. The difference between real and imaginary parts of the refractive index is manifested as optical activity and circular dichroism (CD), that is, the difference in the propagation speed or absorption of the two components. CD has become one of the important expressions of the molecular conformation of biological macromolecules, DNA, and many drug molecules, which is widely used in biology, medicine, chemistry, and other fields [3,4]. However, the inherent CD in natural materials is extremely weak, which requires a high-precision testing system [5].

Metamaterials are new artificial structures composed of subwavelength meta-atoms, which have achieved a variety of electromagnetic manipulation and novel physical phenomena. Metasurfaces are two-dimensional metamaterials that have realized efficient electromagnetic control on extremely small longitudinal scales [6]. Both metamaterials and metasurfaces have achieved broadband or giant chiral optical phenomena, including CD [7,8], chiral wavefront control [9], circular polarization imaging or detection [10,11], and tunable chiral response [12]. In addition, both metasurfaces with or without chirality have been reported for greatly enhancing the CD of chiral molecules [13–15]. In the past 20 years, various chiral phenomena have been observed in metasurfaces includes intrinsic chirality caused by asymmetric meta-atoms and extrinsic chirality caused by achiral structures under oblique incidence [16,17]. The realized functions include spin-selective absorption or reflection

[18,19], polarization rotation, and so on [20–27]. However, these implementations require careful design of asymmetric units or large incident angles, and most of them can only work in a narrow frequency band or cannot achieve arbitrary wavefront control.

In this paper, we propose a new method to achieve chiral optical response based on phase manipulation rather than asymmetry meta-atoms. Simultaneously introducing geometric phase and dynamic phase into an all-silicon metasurface, spin-decoupled phase control of the transmitted terahertz wave is realized. The randomly arranged phase of one of the circularly polarized components causes giant circular dichroism-like effect in transmission. The CD can be controlled by the size of the incident terahertz beam. Not only that, but we also demonstrate another metasurface that achieves arbitrary wavefront control of the circularly polarized wave which is not scattered. This scheme provides a new idea for spin-dependent terahertz wave control.

2. RESULTS AND DISCUSSION

As shown in Fig. 1, the proposed scheme achieves spin-selective transmission of terahertz waves based on phase manipulation. For example, the metasurface shows a randomly distributed phase response for the incident RCP wave, thus generating a transmitted LCP beam with strong divergence. While for the LCP incident wave, all the units in the metasurface cause a same phase shift, so the generated RCP wave will transmit uniformly without introducing additional divergence.

In order to achieve the above functions, design of the metasurface units with spin decoupling function is necessary, so the dynamic phase and geometric phase (Pancharatnam–Berry phase, P-B phase) need to be introduced at the same time. The P-B phase means an additional phase in circularly polarized electromagnetic waves determined by the geometric orientation of the meta-atoms, which appears in anisotropic structures. The P-B phase is spin-dependent, which means the two circular polarization components always obtain opposite phases, while

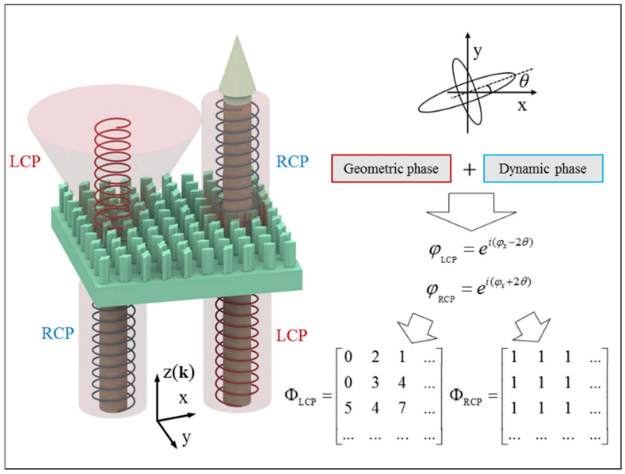

Fig. 1. Schematic diagram of the metasurface which can independently control the phase of two circularly polarized incident waves. The cells are cross-shaped elliptical columns; both the cells and the substrate are made of high-resistance silicon.

the dynamic phase is determined by the geometry of the meta-atom. Assuming that the dynamic phases of the anisotropic element for x and y polarization components are φ_x and φ_y, the geometric phase can be obtained by rotating the element around the z axis by an angle of θ. To achieve the independently controllable circular polarization phase, the dynamic phase and rotation angle of the units need to meet the following equations [28]:

$$\begin{cases} \varphi_x = (\varphi_{RCP} + \varphi_{LCP})/2 \\ \varphi_y = (\varphi_{RCP} + \varphi_{LCP})/2 - \pi \\ \theta = (\varphi_{RCP} - \varphi_{LCP})/4 \end{cases} \quad (1)$$

where φ_{RCP} and φ_{LCP} represent the circular polarization phase response of the metasurface units.

To obtain the metasurface elements with the above-mentioned terahertz response, we used the time-domain finite integration method (CST MICROWAVE STUDIO 2019) to select the geometric parameters of the cross-elliptical silicon columns. In the simulation process, the dielectric constant of intrinsic silicon is set as 11.9, the unit period is $P = 120$ μm, the height is $H = 150$ μm, and the substrate thickness is 350 μm. Both the x and y directions are set as periodic boundaries, and the z boundary near the substrate is excited by a plane wave (linearly polarized), while the other is set as an open boundary. An electric field probe is used above the unit. The cross cylinder is composed of a horizontal (x-axis) ellipse and a vertical (y-axis) ellipse. The short axes of the two elliptical cylinders are $D = 30$ μm, and the long axes are L_x and L_y, respectively. We choose the operating frequency as 1.3 THz. The calculated transmission coefficients and phase shifts of the units when L_x and L_y increased from 30 to 110 μm are shown in Figs. 2(b)–2(e). As shown in the figures, the phase shifts of x- and y-polarized components cover the interval of (−180, 180) degrees within the range of our calculation. Most values of the transmission amplitudes are greater than 0.5, and the maximum value is about 0.7 (the reflection loss of high-resistance silicon itself is about 0.3). In this way, the parameters we choose can make each unit have a consistent high-efficiency transmission amplitude and meet a 360-deg phase shift. Then we select the geometric size values that make the phase values meet Eq. (1), so that the corresponding phases of LCP and RCP waves cover the range of 0–360 deg at an interval of 45 deg. Figures 2(f) and 2(g) show the 64 groups of L_x and L_y values we selected; the transmission amplitudes are all greater than 0.5, and the actual transmission phase differs from the corresponding phase division point by less than 10 deg.

With the above geometric parameters, we can design a spin-decoupled metasurface. Before that, we first determine the phase shift values of the metasurface units for circularly polarized wave, which we called the phase matrix (PM). Without loss of generality, we hope the metasurface has a function of uniform transmission for one of the incident circularly polarized components, while showing a function of diffuse scattering for the other. In order to achieve this goal, we set all the elements in one of the phase matrices to be a value of π/4, and set the other phase matrix to be a set of random numbers (or submatrix with equal elements), as shown in Fig. 3(a). The phase distributions corresponding to the phase matrices (in π/4) are

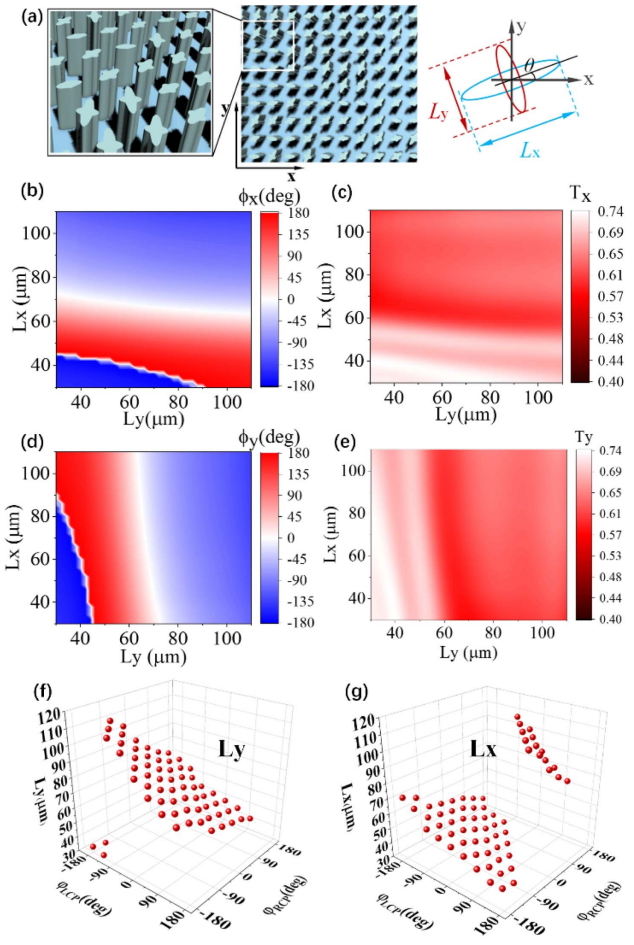

Fig. 2. Simulation and results selection of the geometric parameters of meta-atoms. (a) Schematic diagram of the units. (b)–(e) The transmission amplitudes and phase shifts of the silicon cylinder for x- and y-polarized terahertz waves with different values of L_x and L_y. (f), (g) The selected 64 sets of L_y and L_x values, in which the phases are divided into eight values at intervals of 45 deg.

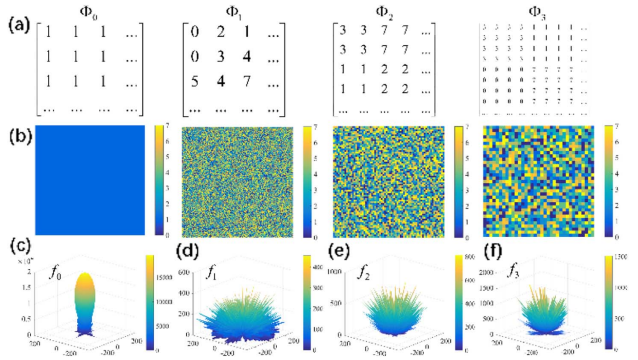

Fig. 3. Phase design of the metasurface with circular dichroism-like effect consists of 140 × 140 units. (a) The phase matrices consist of equal elements or pseudorandom numbers (submatrix with equal elements). (b) The phase distributions corresponding to the phase matrices (in π/4). (c)–(f) Far-field patterns of the metasurfaces with phase distributions of a constant or a random number matrix.

shown in Fig. 3(b). In order to choose a phase matrix for more efficient chiral optical response, we first calculated the far-field pattern corresponding to the above PMs using the following formula [29]:

$$f(\theta,\varphi) = f_e(\theta,\varphi)\sum_{m=1}^{M}\sum_{n=1}^{N}\exp\{-i\{\varphi(m,n) + kD\sin\theta[(m-1/2)\cos\varphi + (n-1/2)\sin\varphi]\}\}, \quad (2)$$

where $f_e(\theta,\varphi)$ is pattern function of a lattice, D is the unit period, M and N are the number of rows and columns of the phase matrix (here $M = N$), and k is the wavenumber.

Figure 3(c) is the far-field pattern of the transmitted wave with a phase matrix of Φ_0, where the incident wave only undergoes a phase shift after passing through the metasurface, and the transmission direction is almost unchanged. According to Figs. 3(d)–3(f), after the incident wave passes through the random phase matrix (Φ_1, Φ_2, Φ_3), the transmitted wave is scattered in almost all directions, and the energy will be dispersed in a large angle range. When monitoring the transmitted wave at a certain point in the far field, only a small amount of energy will be observed. Then a CD-like response of the transmitted wave is obtained. In order to obtain a higher scattering efficiency, we compared the far-field patterns of several phase matrices with different repetition rates, that is, the phase matrix is composed of 1 × 1, 2 × 2, and 4 × 4 identical elements. It can be found that a larger number of repetitions cause a smaller scattering range and efficiency in the far field. Among them, Fig. 3(d) has the highest scattering efficiency.

Based on the geometric parameters in Fig. 2 and the phase matrices of Φ_0 and Φ_1 in Fig. 3, we have designed and processed the metasurface of sample 1. As shown in Fig. 4(a), we use ultraviolet lithography and inductively coupled plasma (ICP) deep silicon etching to form the metasurface units on 500 μm thick high-resistance silicon. A 6.8 μm thick patterned positive photoresist (AZ4620) is obtained as a mask via ultraviolet lithography. Then we use ICP deep silicon etching technology (STS Multiplex ASE-HRM ICP etcher, United Kingdom) to obtain the elliptical elements, and finally the remaining photoresist is washed away to get the final sample. The size of the sample is 2 cm × 2 cm, and the etched area is 1.68 cm × 1.68 cm. Figure 4(a) shows the optical photograph and scanning electron microscope (SEM) image of the sample. Before measuring the terahertz transmission spectrum of the sample, we use commercial software to perform a full-wave simulation of the metasurface. Both the x and y directions are set as open boundaries. A plane wave is placed in the z direction to generate the circularly polarized incident waves. The field monitor is used to obtain the linearly polarized electric field distribution, and then the circularly polarized electric field distribution is obtained through data processing. The transmitted waves in the xoz plane are shown in Fig. 4(b). It can be seen that the transmitted RCP wave propagates uniformly along the $+z$ direction, while the LCP component diverges and propagates in almost all directions.

Figure 4(c) shows the experiment setup for the transmission spectrum measurement of sample 1. We placed four wire grid

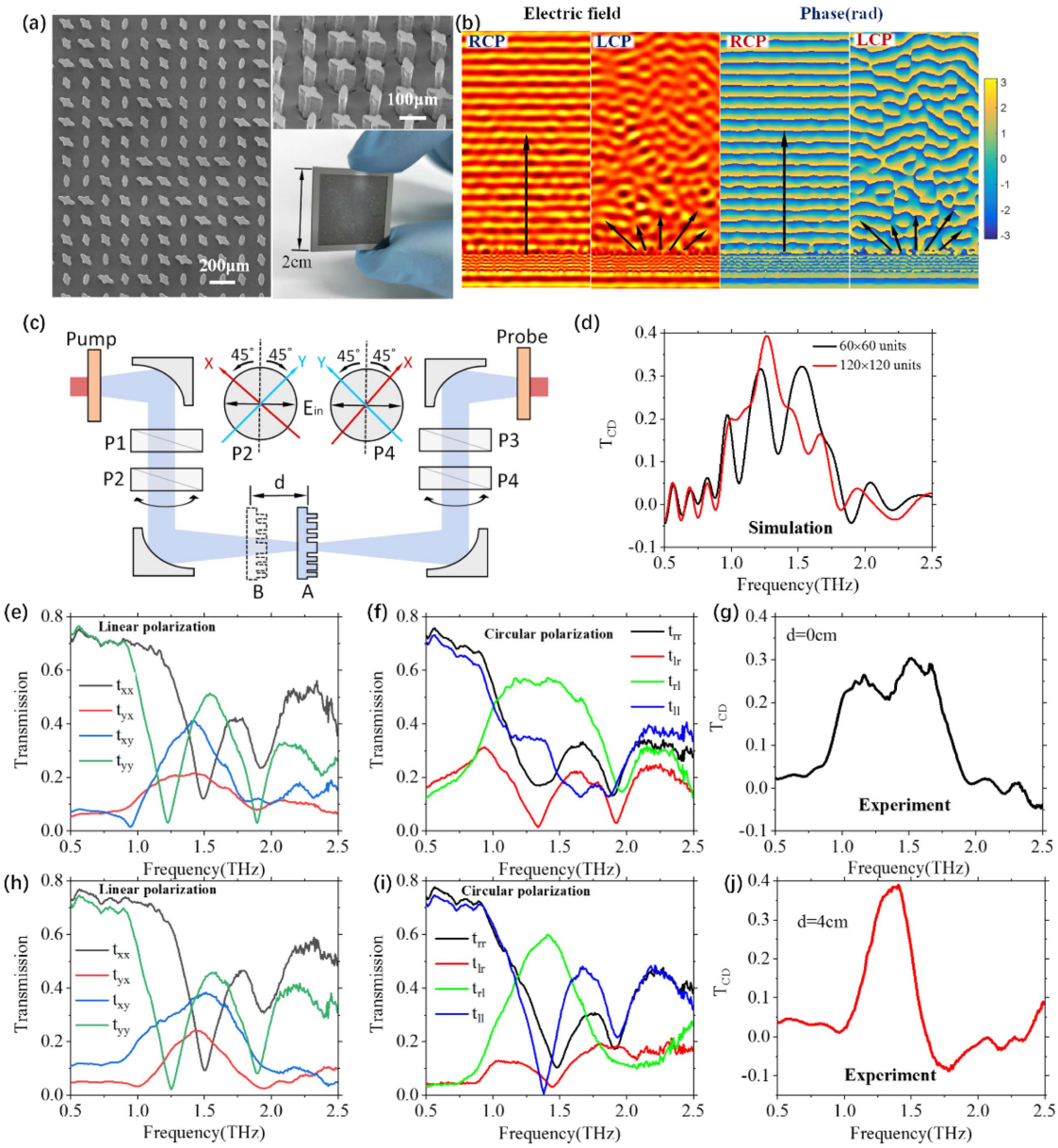

Fig. 4. Morphology characterization and transmission spectrum of the metasurface. (a) Optical photograph and scanning electron microscope (SEM) images of sample 1. (b) Simulated two-dimensional electric field and phase distributions of the transmitted LCP and RCP waves. (c) Terahertz polarization measurement time-domain spectroscopy system. (d) Simulation results of the T_{CD} spectrum for metasurfaces with different numbers of units. (e)–(j) Experiment results of the linear and circular polarization transmission coefficients and T_{CD} spectra.

polarizers in a typical terahertz time-domain spectroscopy system to form a terahertz polarization test system [30]. Among them, the polarizers P1 and P3 are placed on the side close to the emitter and the receiver, respectively, to ensure that the polarization states of the transmitting and receiving waves remain unchanged during the measurement. In addition, P2 and P4 are rotated by ±45 deg (observed along the propagation direction of the terahertz beam) as the x and y coordinate axes of the measurement, as shown by the red and blue arrows in Fig. 4(c). Using the system in the figure, the four transmission coefficients for linear polarization components (t_{xx}, t_{yx}, t_{xy}, and t_{yy}) can be obtained. Then the transmission matrix of circularly polarized waves can be calculated as [31]

$$T_{\text{cir}} = \begin{pmatrix} t_{rr} & t_{rl} \\ t_{lr} & t_{ll} \end{pmatrix} = \frac{1}{2}\begin{pmatrix} t_{xx}+t_{yy}+i(t_{xy}-t_{yx}) & t_{xx}-t_{yy}-i(t_{xy}+t_{yx}) \\ t_{xx}-t_{yy}+i(t_{xy}+t_{yx}) & t_{xx}+t_{yy}-i(t_{xy}-t_{yx}) \end{pmatrix}. \quad (3)$$

We define the transmission difference of the two circular polarization components measured in a certain direction as T_{CD}, which can be calculated by [19]

$$T_{CD} = T_R - T_L = (|t_{rr}|^2 + |t_{lr}|^2) - (|t_{ll}|^2 + |t_{rl}|^2). \quad (4)$$

Since our metasurface is a non-periodic structure, different numbers of cells may produce different circular polarization

responses, thereby achieving tunable CD. In order to verify this function, we place the sample at different positions of the focused terahertz beam during the measurement, so that different numbers of units are illuminated by the terahertz wave. Before that, we first simulated the transmission coefficients of two metasurfaces with 60 × 60 elements and 120 × 120 elements, respectively, in which we placed the electric field probe directly in front of the center of the metasurface. Then we calculated the T_{CD} spectrum in the range of 0.5–2.5 THz using Eq. (4), as shown in Fig. 4(d). It can be found that the maximum value of T_{CD} and the curve width are slightly different in the two cases. The red curve reaches a maximum value of about 0.4 around 1.3 THz, and the peak range is narrow. The maximum value of the black curve is about 0.3, while the curve width is larger. It is worth mentioning that due to the reflection loss of high-resistance silicon, the maximum initial transmission coefficient is about 0.7. The maximum value of T_{CD} is as high as about 0.4, showing a polarization conversion efficiency of about 80%. In order to experimentally verify the circular dichroism of the sample, we use the experiment setup shown in Fig. 4(c) to perform the polarization spectrum measurement of sample 1. First, we place the sample at the focal plane (position A, $d = 0$ cm) of the off-axis parabolic lens, and the measured linear and circular polarization spectra are shown in Figs. 4(e)–4(g). It can be seen in the circularly polarized transmission spectrum that the values of the two co-polarized components (t_{rr} and t_{ll}) are relatively small. For the cross-polarization components, t_{rl} is as high as about 0.55, but t_{lr} is close to zero. Therefore, the calculated T_{CD} value in Fig. 4(g) reaches about 0.3 near 1.4 THz. Then, we moved the sample about 4 cm along the incident direction and placed it in position B for a similar measurement. The results can be seen in Figs. 4(h)–4(j). The diameter of the terahertz beam at position B ($d = 4$ cm) is larger than that at position A, so there will be more units in the sample working. It can be found that the T_{CD} curve in Fig. 4(j) is narrower than that in Fig. 4(g), and the maximum value reaches 0.4 near 1.4 THz. This change rule is consistent with the simulation results in Fig. 4(d), and the tunable CD is obtained. The slight deviation of the working frequency may be caused by the processing deviation of the sample.

In addition to the above-mentioned CD-like effects, the metasurfaces we proposed can also achieve spin-selective wavefront control of terahertz beam. We designed and processed the metasurface of sample 2, and its optical photograph and SEM image are shown in Fig. 5(a). The size of the sample is 1.4 cm × 1.4 cm, and the diameter of the etched area is 8.4 mm (70 units). We set the phase matrix of the incident LCP wave as a focused vortex beam, namely,

$$\tilde{\varphi}_{y1,y2} = \frac{2\pi}{\lambda}\sqrt{r^2 + f^2} \pm 8\theta, \tag{5}$$

where r and θ are the polar axis and angle of the polar coordinates. The focal length $f = 6000$ μm and the topological charge $l = 8$. The phase matrix for the RCP incident wave is a set of random numbers.

We use the terahertz imaging system in Fig. 5(b) to measure the electric field and phase of the transmitted wave. The beam output from the amplified femtosecond laser system (the pulse width is 50 fs, repetition frequency is 1 kHz, and center

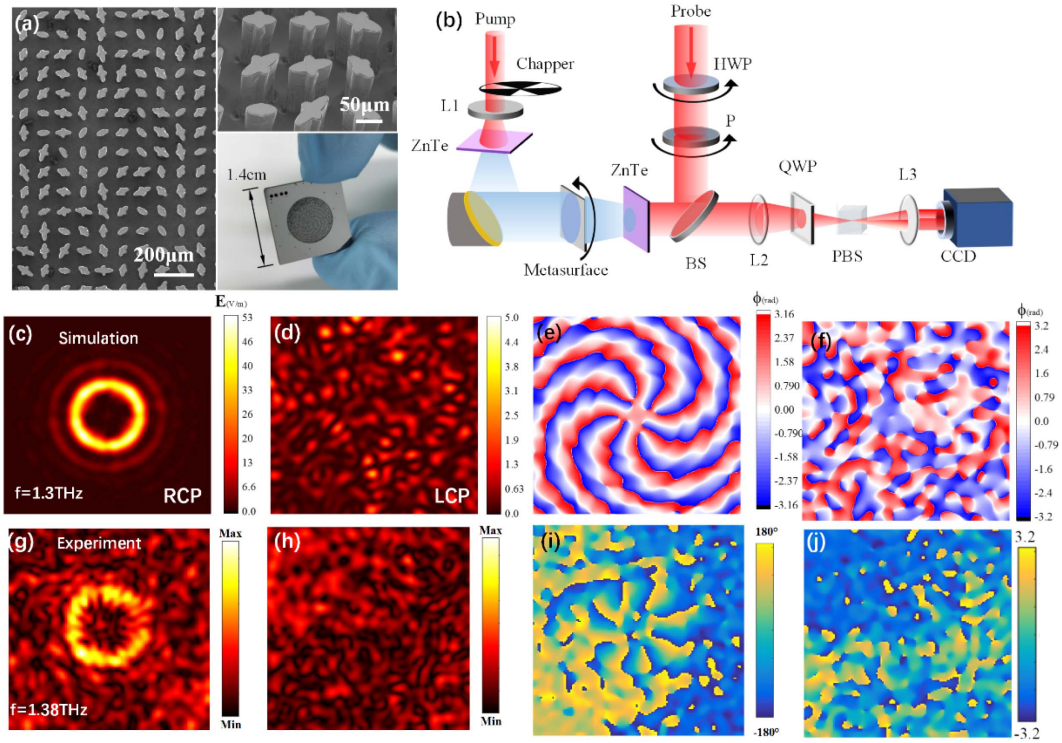

Fig. 5. Spin-selective wavefront control of transmitted terahertz wave using the proposed metasurface. (a) Optical photograph and SEM images of sample 2. (b) Experimental setup of sample 2. (c)–(j) Simulations and measured results of the two-dimensional electric field and phase distributions.

wavelength is 800 nm) is divided into two paths, which are used as the pump beam and probe beam for terahertz imaging. The terahertz wave generated by the ZnTe crystal on the left is vertically polarized (y axis). After passing through the metasurface, the THz wave is irradiated on the crystal on the right and the probe laser beam experiences an electro-optic modulation effect. Then the modulated laser transmits the terahertz electric field image to the CCD camera through the optical imaging system (lenses L2 and L3, quarter-wave plate, and Wollaston prism). During the measurement, the incident and detected terahertz polarization is changed by rotating the sample or the optical polarizer and the half-wave plate at the pump end, and the terahertz electric fields E_{xx}, E_{yx}, E_{yy}, E_{xy} of the four linear polarization components are observed; then the circularly polarized terahertz electric field of the sample can be obtained by Eq. (3).

Before measuring the sample 2, we simulated the transmitted electric field of it with commercial software. Figures 5(c) and 5(d) show the electric fields of the RCP and LCP waves at the focal plane, and Figs. 5(e) and 5(f) show the phase distributions. It can be seen that the RCP component is a vortex beam, while the LCP component is a messy scattered light field. The experimental results at $z = 6000$ μm are shown in Figs. 5(g)–5(j), with a working frequency of 1.38 THz. It can be seen that the measured electric field and phase are basically consistent with the simulation results. It should be pointed out that due to the limitation of the aspect ratio in the etching process, we select the designed etching depth as 150 μm, which results in our optimal design working frequency of about 1.3 THz. More importantly, the actual operating frequency is 1.38 THz due to the processing deviation. The terahertz imaging system we use shows a low signal-to-noise ratio (SNR) at 1.38 THz, which led to the deviation in the results of Fig. 5. Fortunately, we believe that the SNR is still acceptable. This may also show that our scheme has good fabrication tolerance.

3. CONCLUSION

In summary, we propose a new method to achieve giant chiral response of transmitted terahertz waves based on phase control. By introducing geometric phase and dynamic phase at the same time, we designed a spin-decoupled all-silicon terahertz metasurface, which can set different phase matrices for LCP and RCP incident waves. We analyzed the required conditions of the spin-decoupled metasurface elements, and then simulated and selected their geometric parameters. Using the equivalent phase matrix and the random number phase matrix, we achieve the CD-like effect of the transmitted terahertz wave. Simulated and measured results show that the maximum polarization conversion efficiency is about 80%, and the maximum CD value is 0.4. The CD value can be adjusted by the relative position of the sample in the focused terahertz beam. In addition, we also show that this method is used to achieve spin-dependent arbitrary wavefront control. Measurement results of the two-dimensional terahertz electric field are consistent with the simulation results. The proposed method does not require complex asymmetric chiral units, but only needs to set the phase matrix of the metasurface, which is expected to be used in the design of new chiral devices for terahertz wave.

Funding. Basic Research Program of Shenzhen (JCYJ20170412154447469); National Key Research and Development Program of China (2017YFA0700202); National Natural Science Foundation of China (61675147, 61735010, 91838301).

Disclosures. The authors declare no conflicts of interest.

†These authors contributed equally to this work.

REFERENCES

1. L. D. Barron, "True and false chirality and parity violation," Chem. Phys. Lett. **123**, 423–427 (1986).
2. J. Mun, M. Kim, Y. Yang, T. Badloe, J. Ni, Y. Chen, C. W. Qiu, and J. Rho, "Electromagnetic chirality: from fundamentals to nontraditional chiroptical phenomena," Light Sci. Appl. **9**, 139 (2020).
3. Z. Cao, H. Gao, M. Qiu, W. Jin, S. Deng, K. Wong, and D. Lei, "Chirality transfer from sub-nanometer biochemical molecules to sub-micrometer plasmonic metastructures: physiochemical mechanisms, biosensing, and bioimaging opportunities," Adv. Mater. **32**, 1907151 (2020).
4. Y. Tang and A. E. Cohen, "Optical chirality and its interaction with matter," Phys. Rev. Lett. **104**, 163901 (2010).
5. Y. Tang and A. E. Cohen, "Enhanced enantioselectivity in excitation of chiral molecules by superchiral light," Science **332**, 333–336 (2011).
6. N. Yu, P. Genevet, M. A. Kats, F. Aieta, J. Tetienne, F. Capasso, and Z. Gaburro, "Light propagation with phase discontinuities: generalized laws of reflection and refraction," Science **334**, 333–337 (2011).
7. J. K. Gansel, M. Thiel, M. S. Rill, M. Decker, K. Bade, V. Saile, G. Freymann, S. Linden, and M. Wegener, "Gold helix photonic metamaterial as broadband circular polarizer," Science **325**, 1513–1515 (2009).
8. A. Kuzyk, R. Schreiber, Z. Fan, G. Pardatscher, E. Roller, A. Hogele, F. Simmel, A. Govorov, and T. Liedl, "DNA-based self-assembly of chiral plasmonic nanostructures with tailored optical response," Nature **483**, 311–314 (2012).
9. H. Xu, G. Hu, Y. Li, L. Han, J. Zhao, Y. Sun, F. Yuan, G. Wang, Z. Jiang, X. Ling, T. Cui, and C. Qiu, "Interference-assisted kaleidoscopic meta-plexer for arbitrary spin-wavefront manipulation," Light Sci. Appl. **8**, 3 (2019).
10. W. Li, Z. J. Coppens, L. V. Besteiro, W. Wang, A. O. Govorov, and J. Valentine, "Circularly polarized light detection with hot electrons in chiral plasmonic metamaterials," Nat. Commun. **6**, 8379 (2015).
11. L. Kang, S. P. Rodrigues, M. Taghinejad, S. Lan, K. Lee, Y. Liu, D. H. Werner, A. Urbas, and W. Cai, "Preserving spin states upon reflection: linear and nonlinear responses of a chiral meta-mirror," Nano Lett. **17**, 7102–7109 (2017).
12. T. Kim, S. Oh, H. Kim, H. Park, O. Hess, B. Min, and S. Zhang, "Electrical access to critical coupling of circularly polarized waves in graphene chiral metamaterials," Sci. Adv. **3**, e1701377 (2017).
13. J. Guirado, M. Svedendahl, and J. Puigdollers, "Enhanced chiral sensing with dielectric nanoresonators," Nano Lett. **20**, 585–591 (2020).
14. L. D. Barron, N. Gadegaard, and M. Kadodwala, "Ultrasensitive detection and characterization of biomolecules using superchiral fields," Nat. Nanotechnol. **5**, 783–787 (2010).
15. W. Zhang, T. Wu, R. Wang, and X. Zhang, "Amplification of the molecular chiroptical effect by low-loss dielectric nanoantennas," Nanoscale **9**, 5701–5707 (2017).
16. E. Plum, V. A. Fedotov, and N. I. Zheludev, "Metamaterials: optical activity without chirality," Phys. Rev. Lett. **102**, 113902 (2009).
17. I. Sersic, M. A. Haar, F. B. Arango, and A. F. Koenderink, "Ubiquity of optical activity in planar metamaterial scatterers," Phys. Rev. Lett. **108**, 223903 (2012).
18. L. Jing, Z. Wang, R. Maturi, B. Zheng, H. Wang, Y. Yang, L. Shen, R. Hao, W. Yin, E. Li, and H. Chen, "Gradient chiral metamirrors for spin-selective anomalous reflection," Laser Photonics Rev. **11**, 1700115 (2017).

19. Z. Wang, H. Jia, K. Yao, W. Cai, H. Chen, and Y. Liu, "Circular dichroism metamirrors with near-perfect extinction," ACS Photonics **3**, 2096–2101 (2016).
20. F. Neubrech, M. Hentschel, and N. Liu, "Reconfigurable plasmonic chirality: fundamentals and applications," Adv. Mater. **32**, 1905640 (2020).
21. D. C. Hooper, A. G. Mark, C. Kuppe, J. T. Collins, P. Fischer, and V. K. Valev, "Strong rotational anisotropies affect nonlinear chiral metamaterials," Adv. Mater. **29**, 1605110 (2017).
22. C. Niu, Z. Wang, J. Zhao, L. Du, N. Liu, Y. Liu, and X. Li, "Photonic heterostructures for spin-flipped beam splitting," Phys. Rev. Appl. **12**, 044009 (2019).
23. J. Fan, Y. Cheng, and B. He, "High-efficiency ultrathin terahertz geometric metasurface for full-space wavefront manipulation at two frequencies," J. Phys. D **54**, 115101 (2021).
24. Y. Cheng, F. Chen, and H. Luo, "Multi-band giant circular dichroism based on conjugated bilayer twisted-semicircle nanostructure at optical frequency," Phys. Lett. A **384**, 126398 (2020).
25. Y. Cheng, J. Fan, H. Luo, and F. Chen, "Dual-band and high-efficiency circular polarization convertor based on anisotropic metamaterial," IEEE Access **8**, 7615–7621 (2020).
26. J. Fan and Y. Cheng, "Broadband high-efficiency cross-polarization conversion and multi-functional wavefront manipulation based on chiral structure metasurface for terahertz wave," J. Phys. D **53**, 025109 (2020).
27. Y. Li, Y. Li, L. Chen, and M. Hong, "Reflection tuning via destructive interference in metasurface," Opto-Electron. Eng. **44**, 313–318 (2017).
28. J. P. B. Mueller, N. A. Rubin, R. C. Devlin, B. Groever, and F. Capasso, "Metasurface polarization optics: independent phase control of arbitrary orthogonal states of polarization," Phys. Rev. Lett. **118**, 113901 (2017).
29. T. J. Cui, M. Q. Qi, X. Wan, J. Zhao, and Q. Cheng, "Coding metamaterials, digital metamaterials and programmable metamaterials," Light Sci. Appl. **3**, e218 (2014).
30. W. Choi, G. Cheng, Z. Huang, S. Zhang, T. B. Norris, and N. A. Kotov, "Terahertz circular dichroism spectroscopy of biomaterials enabled by kirigami polarization modulators," Nat. Mater. **18**, 820–826 (2019).
31. C. Menzel, C. Rockstuhl, and F. Lederer, "Advanced Jones calculus for the classification of periodic metamaterials," Phys. Rev. A **82**, 053811 (2010).